Journal of Applied Polymer Science

Effects of Nucleating Agents on the Morphologies and Performances of Poly(vinylidene fluoride) Microporous Membranes via Thermally Induced Phase Separation

Min Liu,[1,2] Dong-Gen Chen,[1] Zhen-Liang Xu,[1,2] Yong-Ming Wei,[1] Meng Tong[2]

[1]State Key Laboratory of Chemical Engineering, Membrane Science and Engineering R&D Lab, Chemical Engineering Research Center, East China University of Science and Technology, 130 Meilong Road, Shanghai 200237, China

[2]Shanghai Key Laboratory of Advanced Polymeric Materials, Key Laboratory for Ultrafine Materials of Ministry of Education, School of Materials Science and Engineering, East China University of Science and Technology, 130 Meilong Road, Shanghai 200237, China

Correspondence to: Z.-L. Xu (E-mail: chemxuzl@ecust.edu.cn)

ABSTRACT: The effects of nucleating agents on the morphology and performance of poly(vinylidene fluoride) (PVDF) microporous membranes via thermally induced phase separation were investigated. The nucleating agents studied were dicyclohexyl benzene amide (TMB-5), 2,2-methylene bis(4,6-tertiary butyl phenol) sodium phosphate (TMP-1), and 1,3 : 2,4-di-*p*-methylbenzylidene sorbitol (DM–LO). Light transmittance experiments and differential scanning calorimetry (DSC) were performed to obtain phase diagrams of PVDF/tributyl citrate/di(2-ethylhexyl) phthalate/nucleating agent doped solutions. The morphology and performance of the prepared PVDF microporous membranes were characterized with scanning electron microscopy and microfiltration experiments. The results show that the thermodynamics of liquid–liquid phase separation were not affected by the addition of the nucleating agents, but solid–liquid phase separation was influenced. The system with 0.3 wt % TMB-5 had the fastest crystallization rate and a better nucleation ability. The PVDF microporous membranes had a partly closed, lacy bicontinuous structure with TMP-1 and DM–LO, whereas the membrane with 0.3 wt % TMB-5 had an interconnected bicontinuous structure. The pore size distribution became narrower with the addition of nucleating agent. With 0.3 wt % TMB-5, the membrane had the minimum mean pore size (0.095 μm), a porosity of 80.3%, and a pure water flux of 270 $L \cdot m^{-2} \cdot h^{-1}$; these values were higher than those of the pure PVDF membrane. The performances of the membranes decreased with additions of TMB-5 of greater than 0.3 wt %. © 2012 Wiley Periodicals, Inc. J. Appl. Polym. Sci. 000: 000–000, 2012

KEYWORDS: membrane; morphology; phase separation; nucleation

Received 23 June 2011; accepted 18 June 2012; published online
DOI: 10.1002/app.38234

INTRODUCTION

Since the thermally induced phase separation (TIPS) method was first introduced by Castro[1] in the 1980s, it has gained a lot of attention.[2–11] During the TIPS process, the polymer/diluent solution undergoes solid–liquid (S–L) or liquid–liquid (L–L) phase separation with subsequent polymer crystallization. The final morphology of the membrane depends on the thermodynamics and dynamics of phase separation. If the polymer–diluent interaction is strong, S–L phase separation occurs, which leads to the formation of a spherulitic structure.[2] The membrane structure is mainly determined by the thermodynamics of phase separation, and the dynamics of phase separation only affect the size of the spherulites. If the polymer–diluent interaction is weak, L–L phase separation with subsequent polymer crystallization occurs when the polymer concentration is lower than the monotectic point. However, the final morphology of the membrane depends on the dynamics and thermodynamics of phase separation. Generally, a membrane is formed by a nucleation–growth mechanism at a slow cooling rate; this leads to the formation of a partly closed cellular pore structure. Thus, membrane formation undergoes a spinodal decomposition mechanism under quenching conditions; this leads to a bicontinuous structure. Although L–L phase separation follows by solidification of the polymer, the bicontinuous membrane structure can be produced by the control of crystallization kinetics.[3] Because it is difficult to find, a single diluent can dissolve the polymer at high temperature, and then, the polymer/diluent solution undergoes L–L phase separation in thermodynamics. Therefore, a mixed diluent is applied to control the membrane-formation mechanism and is a convenient and practical method.

Some researchers have reported poly(vinylidene fluoride) (PVDF) membranes prepared via TIPS. Most of the studies have been focused on polymer solutions with a single diluent;[12–15] whereas few investigators[16–20] have reported polymer/mixed diluent systems. Our research group prepared PVDF microporous membranes via the TIPS method with a single and mixed diluent.[21,22] The previous results show that the morphology of the PVDF membranes is influenced by the thermodynamic compatibility between the polymer and diluent, the polymer concentration, the cooling conditions, and so on. It was found that the bicontinuous structure of the PVDF membranes prepared by a mixed diluent, which is a typical membrane structure produced by a system with an L–L phase separation with subsequent polymer crystallization, formed only a thin layer near the surface. There was no such morphology in the whole cross section of the membrane, although the L–L phase separation appeared and quenching conditions were applied in the cooling process.[16,17,22]

Deeprasertkul[23] reported that nucleating agents (talc, calcium carbonate, and cyclodextrin) could be directly added to initiate faster crystallization and gave a smaller spherulite size for poly(lactic acid) and its blend with natural rubber. Cramez et al.[24] found that the compounding of polypropylene (PP) with nucleating agents (a red pigment, sodium benzoate, and a mixture of pimelic acid and calcium stearate) resulted in a very fine microstructure in clear contrast with the very coarse one formed with the pure PP. Also, a few researchers[25–27] have reported that the morphology of PP or poly(phenylene sulfide) membranes resulted not only from the aforementioned factors (polymer concentration, cooling conditions, mixed diluent composition, and coarsening) but also from nucleating agents. Smith et al.[28] successfully prepared asymmetric microporous PVDF articles by the TIPS method with nucleating agents (perylene pigments and nanometer sized particles of polytetrafluoroethylene). A polymer crystals with a center of nucleating agents is called *heterogeneous nucleation*. Because of the enhancement of the crystal nucleus, the crystallization rate increases, and the sizes of the spherulites decrease; the morphology and performances of the membranes change consequently. The nucleating agents play an important role in the dynamics of phase separation for the preparation of microporous membranes via TIPS.

The purpose of this study was to investigate the effects of nucleating agents on PVDF microporous membranes via TIPS. Dicyclohexyl benzene amide (TMB-5), 2,2-methylene bis(4,6-tertiary butyl phenol) sodium phosphate (TMP-1), and 1,3 : 2,4-di-*p*-methylbenzylidene sorbitol (Irgaclear DM–LO) were used as nucleating agents. To our best knowledge, this is the first time that the direct use of these three nucleating agents on the morphology and performance of PVDF membranes via TIPS has been reported. We focused on the effects of the nucleating agent type and amount on the membrane-formation mechanism and membrane structure on the PVDF/tributyl citrate (TBC)/di(2-ethylhexyl) phthalate (DEHP) system. Moreover, the performance of the PVDF membranes is discussed in detail.

EXPERIMENTAL

Materials

PVDF (Solef6010, weight-average molecular weight = 166,000, weight-average molecular weight/number-average molecular weight = 1.7) was supplied by Solvay Advanced Polymers, LLC, Brussels (Belgium). TBC (density = 1.039 g/cm^3, boiling point = 170°C, 133.3 Pa), DEHP (density = 0.983 g/cm^3, boiling point = 386°C), ethanol, and hexane were purchased from Shanghai Chemical Reagent Co. The nucleating agents were Irgaclear DM–LO [melting point (T_m) $\geq$ 255°C, Ciba Specialty Chemicals], TMB-5 ($T_m \geq$ 340°C, Shanxi Institute of Chemical Industry) and TMP-1 ($T_m \geq$ 350°C, Shanxi Institute of Chemical Industry). The extraction solvents were ethanol and hexane. All chemicals were used without purification.

Table I. Dope Solution Compositions of the Various PVDF/TBC/DEHP Systems with Nucleating Agent

			Nucleating agent	
System	Membrane	PVDF (wt %)	Type	Content (wt %)
NA0	M0	30	TMB-5	0
NA1-1	M1-1	30	TMB-5	0.1
NA1-3	M1-3	30	TMB-5	0.3
NA1-5	M1-5	30	TMB-5	0.5
NA1-10	M1-10	30	TMB-5	1.0
NA2	M2	30	TMP-1	0.3
NA3	M3	30	DM-LO	0.3

Preparation of the PVDF/TBC/DEHP Systems with Nucleating Agents and Membranes

A mixture of TBC (30 wt %) and DEHP (70 wt %) were premixed as the mixed diluent. Measured amounts of PVDF, mixed diluent, and nucleating agent were mixed in a glass vessel heated to 200°C for 30 min until PVDF was completely dissolved in the diluent. The homogeneous solution was quenched in ice water to solidify it; this yielded a solid PVDF/TBC/DEHP/nucleating agent sample. The dope solution compositions of various PVDF/TBC/DEHP systems with nucleating agents are given in Table I. The solid sample was sliced into small pieces and melted again to obtain a homogeneous PVDF/TBC/DEHP/nucleating agent solution. The dope solution was cast onto an alloyed plate (a square with a side length of 150 mm and a thickness of 2 mm) at 220°C by a casting knife with a gap of 350 μm and then quenched quickly in a water bath (20°C). The diluent in the membrane was extracted with ethanol for 48 h to ensure complete diluent removal. The ethanol was refreshed at least three times. Then, the wet membrane was formed. Subsequently, ethanol in the wet membrane was extracted with hexane, and the hexane was evaporated in open air to produce the dry membrane.

Phase Diagram

The cloud point (T_{cloud}) was measured according to the method reported by Lloyd et al.[3] The light transmittance measurement experiments were carried out by a self-made device, the schematics of which are described in our previous article.[22] The prepared small pieces of solid sample were heated on a hot stage at 220°C for 3 min to ensure homogeneity of the melt. Subsequently, the sample was cooled to 50°C at a rate of 10°C/min to induce phase separation. The experiment was conducted with a

collimated laser. The intensity of the transmitted light decreased as L–L phase separation occurred. The onset of the signal change was taken as an indication of the onset of L–L phase separation.

The crystallization temperature (T_c) was determined with a differential scanning calorimeter (PerkinElmer Diamond DSC instrument, Waltham Massachusetts (USA)). All of the measurements were performed under a nitrogen atmosphere, and the samples weighed about 8 mg. The preparation of a microporous membrane via the TIPS process is a nonisothermal process. Therefore, the nonisothermal crystallization behavior of PVDF in the diluent was studied on the PerkinElmer Diamond DSC instrument. The solid sample was melted at 200°C for 5 min to erase the thermal history, cooled to 50°C at a rate of 10°C/min, and then heated to 200°C at a rate of 10°C/min again. The onset temperatures of the exothermic peak during cooling and the endothermic peak during heating were taken as T_c and T_m, respectively. The crystallization peak temperature was abbreviated as T_c^{peak}. The degree of supercooling (ΔT_c) was the difference between T_m and T_c.

The relative degree of crystallization as a function of temperature [$X(T)$] is defined as follows:

$$X(T) = \frac{\int_{T_0}^{T} (dH_C/dT)dT}{\int_{T_0}^{T_\infty} (dH_C/dT)dT} \quad (1)$$

where T_0 and T_∞ are the onset and end crystallization temperatures, respectively, and dH_C/dT is the heat flow rate. In nonisothermal crystallization, time t is related to temperature T as follows:

$$t = \frac{T_0 - T}{\Phi} \quad (2)$$

where T is the temperature at time t, T_0 is the temperature at which crystallization begins ($t = 0$), and Φ is the cooling rate.[18]

The development of the relative crystallization with time was gained according to eq. (1) and eq. (2). The *crystallization half-time* ($t_{1/2}$) is defined as the time at which the relative crystallization degree is 50%.

Membrane Characterization

Membrane Morphology. The dry membrane was fractured in liquid nitrogen and deposited on a copper holder. All samples were coated with gold *in vacuo*. The morphology of the membranes was examined with scanning electron microscopy (SEM; JEOL model JSM-6360 LV, Tokyo, Japan).

Permeation Performance. A self-made dead-end stirred cell (effective area = 1.134×10^{-3} m^2) was used to measure the pure water permeation flux (PWP) of the PVDF membranes, and the schematics were described in our previous article.[29] The newly prepared wet membranes were prepressured at 0.1 MPa with pure water for 0.5 h before measurement, and then, PWP was measured. PWP was defined as follows:

$$\mathrm{PWP} = \frac{Q}{A} \quad (3)$$

where Q is the flux per unit time (L/h) and A is the effective area of the membrane (m^2).

Porosity. The porosity (ϵ) is defined as the volume of the pores divided by the total volume of the porous membrane. It is usually determined by the gravimetric method by determination of the weight of liquid (here ethanol) contained in the membrane pores:

$$\varepsilon = \frac{(m_1 - m_2)/\rho_{\mathrm{ethanol}}}{(m_1 - m_2)/\rho_{\mathrm{ethanol}} + m_2/\rho_p} \quad (4)$$

where m_1 is the weight of the wet membrane (g), m_2 is the weight of the dry membrane (g), ρ_{ethanol} is the ethanol density (0.790 g/cm^3), and ρ_p is the polymer density (1.780 g/cm^3).[22]

Pore Size Distribution. The pore size distribution was determined by the gas bubble pressure method.[30] The newly prepared wet membrane was used to measure the pore size distribution. Namely, the membrane pores was completely wetted with ethanol at the beginning of experiment. Compressed air was used to generate the applied pressure. To construct the flow–pressure curve for a wet membrane, the wet membrane was loaded into the cell of a self-made apparatus, details of which can be found in a previously published article.[31] The pressure drop across the membrane (P) was increased slowly until flow was detected. P was taken to be the minimum pressure. Namely, the largest pores in the membrane were opened. As successively higher P values were applied, the volume flow rate of the wet membrane was read from the flow meter. When all of the pores of the membrane were opened, continuous increases in P caused corresponding linear increases in the flow. Subsequently, the dry membrane flow–pressure curve was constructed as successively lower pressures were applied. All experiments were carried out at room temperature. The pressure increased from 0.1 to 0.6 MPa and then decreased to 0.1 MPa at intervals of 0.005 MPa. The effective area of the membrane was 6.154×10^{-4} m^2. The report values were the average value of three samples. The pore size distribution, mean pore size (r_m), maximum pore size ($r_{\max}$), and minimum pore size ($r_{\min}$) could be determined from a statistical method.[31–33]

The pore size distribution [$f(r)$] is defined as follows:

$$f(r) = \frac{d[F_W(r)/F_D(r)]}{dr} \quad (5)$$

where $F_W(r)$ is the gas flow of the wet membrane (cm^3/s) and $F_D(r)$ is the gas flow of the dry membrane (cm^3/s). The pore size (r) could be described by Laplace's equation:

$$r = \frac{2\sigma\cos\theta}{P} \quad (6)$$

where σ is the surface tension of ethanol (22.8×10^{-3} N/m), θ is the contact angle of ethanol to membrane (°), and P is the pressure drop across the membrane (Pa).

RESULTS AND DISCUSSION

Phase Diagram

As shown in Table II, the phase-separation temperatures for the PVDF/TBC/DEHP systems with nucleating agents, including

Table II. Effects of Different Nucleating Agents on the Phase-Separation Temperature

System	Nucleating agent		T_{cloud} (°C)	T_c (°C)	T_c^{peak} (°C)	T_m (°C)	$t_{1/2}$ (min)	ΔT_c (°C)
	Type	Content (wt %)						
NA0	—	0	200.0	139.7	136.8	156.2	1.2	16.5
NA1-3	TMB-5	0.3	199.6	141.9	139.7	159.0	0.9	17.1
NA2	TMP-1	0.3	200.7	140.6	138.2	156.0	1.0	15.4
NA3	DM-LO	0.3	199.7	140.8	138.6	158.4	0.9	17.6

TMB-5, TMP-1, and DM–LO, respectively, indicated the effects of nucleating agent type on the phase-separation behavior. T_{cloud} (L–L phase-separation temperature) was almost the same in the blending systems with the nucleating agent (NA1-3, NA2, and NA3) or without a nucleating agent (NA0). This means that the addition of different types of nucleating agent showed no effects on the L–L phase separation. This was because T_{cloud} was mainly associated with the thermodynamics of the blending system.

As shown in Figure 1, the crystallization peak with the addition of nucleating agent shifted to higher temperatures, and the shape of the peak became more sharp because of the heterogeneous nucleation. System NA1-3 had the highest T_c (141.9°C), T_c^{peak} (139.7°C), and T_m (159.0°C) and the smallest $t_{1/2}$ (0.9 min) of the four systems shown in Table II. The smaller $t_{1/2}$ was, the faster the crystallization rate was. Despite the fact that $t_{1/2}$ of system NA3 was also 0.9 min, the nucleation ability of DM–LO was weaker than that of TMB-5 because of its higher ΔT_c. System NA2 had a better nucleation effect (ΔT_c = 15.4), but it had a longer $t_{1/2}$ (1.0 min) and lower T_c and T_m. Accordingly, system NA1-3 had a better nucleation effect and the fastest crystallization rate when it was cooled under the same cooling conditions. The results suggest that TMB-5 acted as good nucleating agent for the PVDF/TBC/DEHP dope solution.

The phase diagram for the PVDF/TBC/DEHP systems with different contents of TMB-5 is shown in Figure 2. The effects of the nucleating agent amount on the phase-separation behavior are displayed. T_{cloud} changed little with increasing nucleating agent content. This indicated that the contents of nucleating agent showed no effects on the thermodynamics of L–L phase separation.

The DSC cooling curves of PVDF/TBC/DEHP systems with different contents of TMB-5 are presented in Figure 3. The crystallization peak shifted to higher temperatures from 0 to 0.3 wt % TMB-5 and then shifted to low temperatures from 0.3 to 1.0 wt % TMB-5. T_c (141.9°C) reached its peak value and the width of crystallization peak was the narrowest with a content of 0.3 wt % TMB-5. From these results, it is clear that the crystallization rate of PVDF increased significantly with the addition of 0.3 wt % TMB-5. Thus, a suitable dosage of TMB-5 was 0.3 wt %, which showed the best nucleating effects.

Effects of Different Nucleating Agents on the Morphologies of the PVDF Microporous Membranes

With different nucleating agents in the PVDF/TBC/DEHP systems, PVDF membranes were prepared by the TIPS process. The micrographs of the cross sections are shown in Figure 4. The PVDF membrane without nucleating agent (M0; Figure 4) presented a bicontinuous structure, which resulted from L–L phase separation. However, only a thin layer near the upper surface of the membrane was observed. Meanwhile, a deformed spherulitic structure was observed in the other part of the membrane cross section. This morphology was a bicontinuous-like structure (part bicontinuous and part spherulitic). This phenomenon was due to different cooling rates of the membrane at the upper and bottom surfaces of the membrane.[22] In addition,

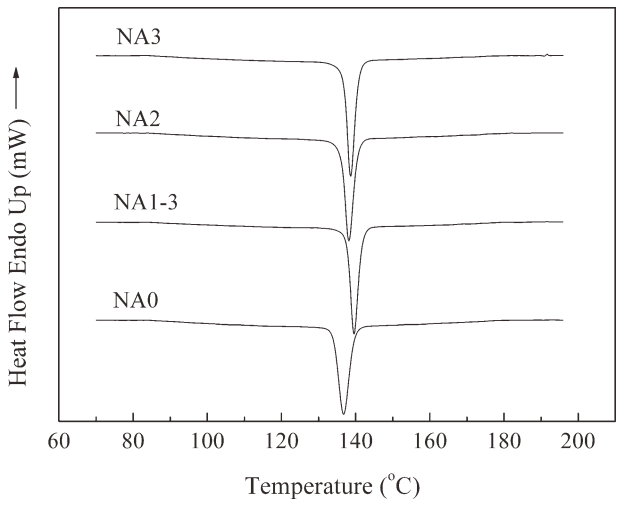

Figure 1. DSC cooling curves of PVDF/TBC/DEHP systems with different nucleating agents.

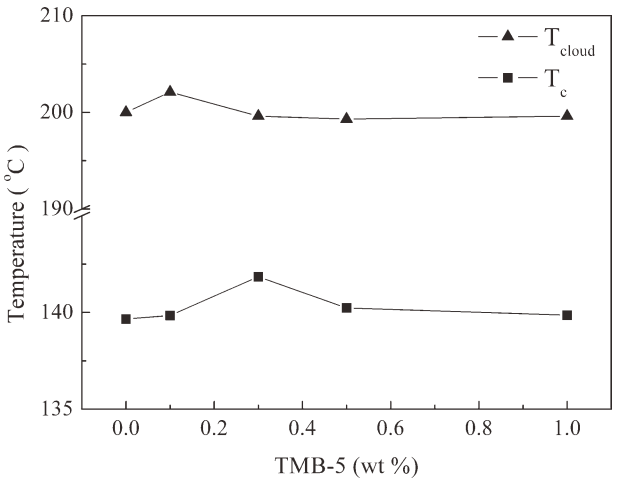

Figure 2. Phase diagram of PVDF/TBC/DEHP systems with different nucleating agent contents.

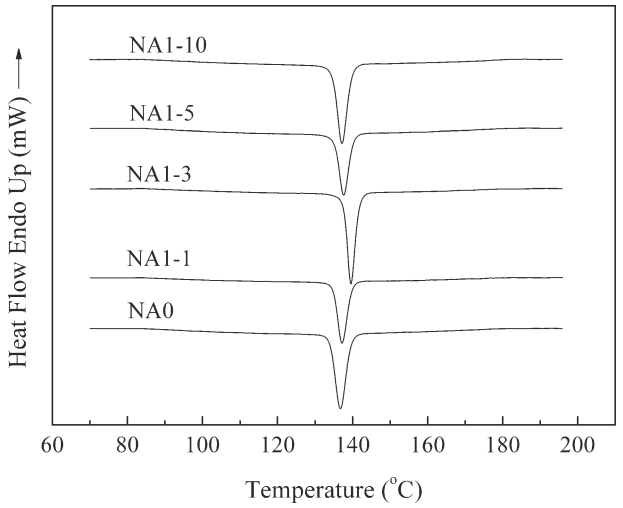

Figure 3. DSC cooling curves of PVDF/TBC/DEHP systems with different nucleating agents contents.

as the temperature decreased to T_o, L–L phase separation completed. Then phase separation entered S–L separation, and the crystallization mechanism of the polymer-rich phase was homogeneous nucleation. The spherulite dimension was large, and the crystallization rate of PVDF in the rich phase was slow. Therefore, a typical deformed spherulitic structure was present in the cross section.

However, for PVDF membranes with three different nucleating agents, including TMB-5, TMP-1, and DM–LO, respectively, uniform bicontinuous structures were observed in the whole cross section, as shown in Figure 4 (M1-3, M2, and M3). From the previously analysis, it was known that there was no effect of nucleating agent type on the thermodynamics of L–L phase separation in the process of membrane preparation. However, the presence of the nucleating agents greatly affected the crystallization dynamics of PVDF. In heterogeneous nucleation, the nucleating agent helps lower the free-energy barrier and, thus, favors faster nucleation. Therefore, nucleating agents act as nuclei, which lead to increases in the nucleation density and crystallization rate. Consequently, the sizes of the spherulites decrease greatly. Therefore, the PVDF membranes showed a homogeneous bicontinuous structure.

According to the enlarged cross-sectional micrographs of the membranes with the three types of nucleating agents, the morphology of membrane M1-3 was different from those of membranes M2 and M3. Membrane M1-3 presented an interconnected bicontinuous structure. Membranes M2 and M3 presented a partly closed, lacy bicontinuous structure. It may have been that the nucleation mechanism and nuclei size of TMP-1 and DM–LO were different from those of TMB-5. Therefore, the morphologies of membranes M2 and M3 differed from that of membrane M1-3.

Effects of the Nucleating Agent Content on the Morphologies of the PVDF Microporous Membranes

As shown in Figure 5, the contents of nucleating agent were 0.1, 0.3, 0.5, and 1.0 wt %, respectively. As shown in Figure 4 (M0), the bicontinuous-like structure was clear for the PVDF membrane without a nucleating agent. As discussed previously, there were no effects of nucleating agent content on the thermodynamics of L–L phase separation. Therefore, with different contents of the nucleating agent TMB-5, the membranes all presented a bicontinuous structure, as shown in Figure 5. When the nucleating agent content was 0.1 wt %, the membrane structure was similar to homogeneous, as shown in Figure 5 (M1-1), but the deformed spherulitic structure still existed, and a spherulite boundary was visible, although it was not very clear.

Thus, the PVDF membranes with 0.3 wt % TMB-5 showed a homogeneous interconnected bicontinuous structure, as shown in Figure 5 (M1-3). This was because of the increase of heterogeneous nuclei and because the spherulites were impinged in a small space with the addition of nucleating agent. The limited growth space of spherulites led to the smaller spherulite. With the addition of 0.3 wt % TMB-5, the crystallization rate and T_c were the highest (as shown in Table II and Figures 2 and 3), and then, the interconnected bicontinuous membrane structure was present, as shown in Figure 5 (M1-3). With a content of nucleating agent of 0.5 wt % TMB-5, the membrane structure was similar to that of M1-3 but with a slight coarseness. Furthermore, as shown in Figure 5 (M1-10), the PVDF membrane with 1.0 wt % TMB-5 showed a partly closed, lacy bicontinuous structure. This was attributed to the excessive dosage of nucleating agent, which aggregated together as one multinucleus, and the growth environments of the spherulites changed.

Permeation Performance and Pore Size

It is known that several factors, including membrane morphology, pore size, and porosity together determine the permeation flux of a membrane. The permeation performance is influenced by the addition of nucleating agent, which influences the membrane morphology. The relationship of the PWP and porosity of the membranes against the nucleating agent type and content is shown in Table III. First, with regard to the PWP, the flux of the membranes with the nucleating agent TMB-5 increased from 0.1 to 0.3 wt % TMB-5 and then decreased from 0.3 to 1.0 wt % TMB-5. Generally, the PWP reached a maximum value of 270 $L{\cdot}m^{-2}{\cdot}h^{-1}$ when the TMB-5 content was 0.3 wt %. With the same nucleating agent content of 0.3 wt %, the flux increased in the following sequence: M1-3 < M2 < M3. This was related to the porosity and pore size. Second, with different contents of the nucleating agent TMB-5, the porosity of the membrane reached the maximum value at 0.3 wt %. With increasing nucleating agent dosage greater than 0.3 wt %, the porosity decreased. This was because the membranes M1-5 and M1-10 presented a coarse or partly closed, lacy bicontinuous structure, as shown in Figure 5 (M1-5 and M1-10); this was attributed to the excessive nucleating agent dosages. Lastly, when the nucleating agent content was 0.3 wt %, the porosity of membrane M1-3 was 80.3%, which was the largest among the three membranes, M1-3, M2, and M3. This may have been because the membrane M1-3 presented an interconnected, bicontinuous structure, whereas membranes M2 and M3 presented a partly closed, lacy bicontinuous structure, as shown in

Applied Polymer SCIENCE

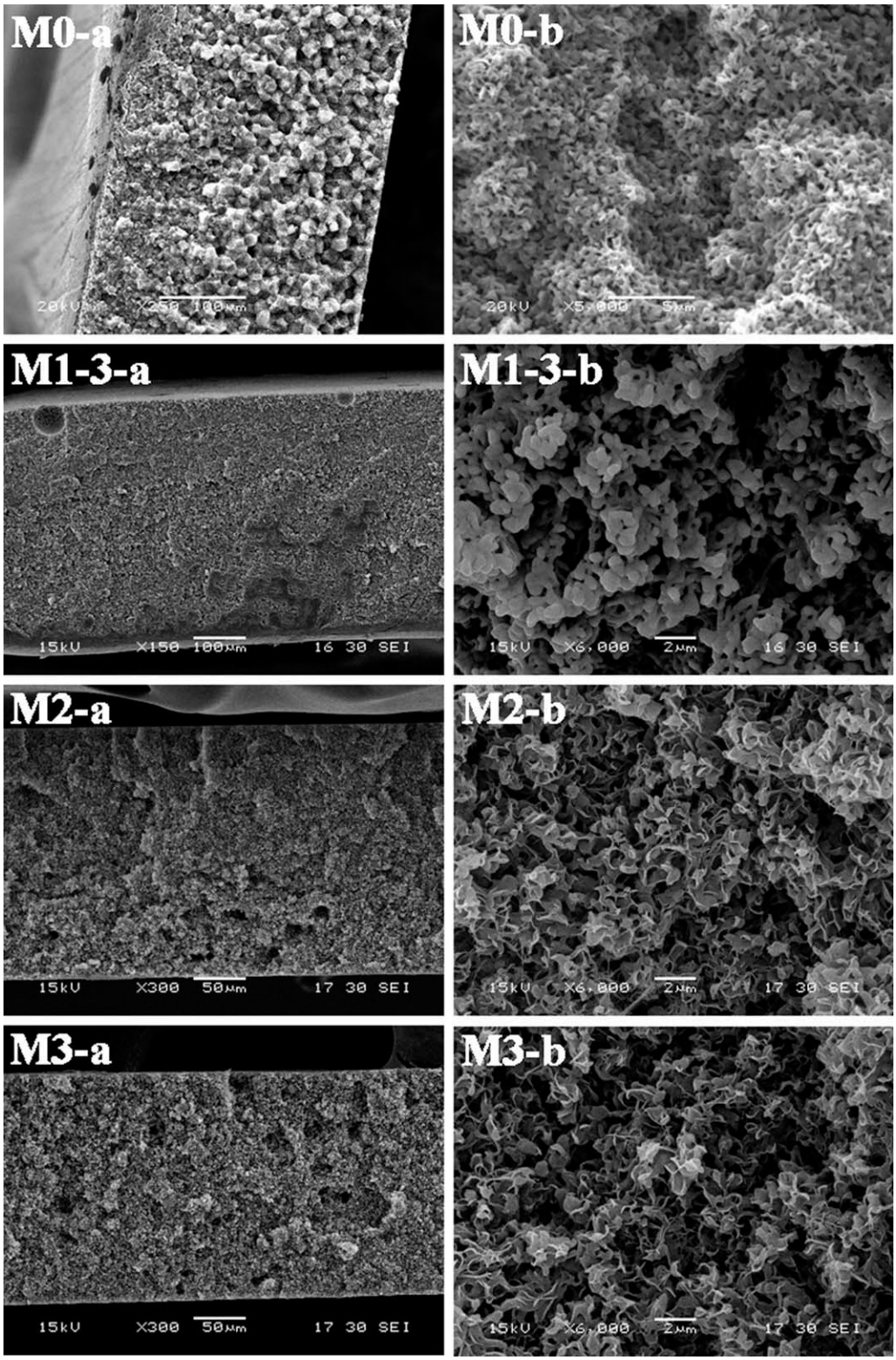

Figure 4. SEM micrographs of PVDF membranes with different nucleating agents: (a) whole and (b) enlarged cross sections.

Figure 4 (M1-3, M2, and M3). Moreover, the porosities of membranes M2 and M3 were lower than that of membrane M0 (without a nucleating agent). The high flux values of M2 and M3 may have been due to the dimension of pore size.

The pore size information of the prepared membranes is listed in Figure 6 and Table IV. It was obvious that the mean pore size of the membranes with the addition of TMB-5 was smaller than that of membrane M0. The mean pore sizes of membranes

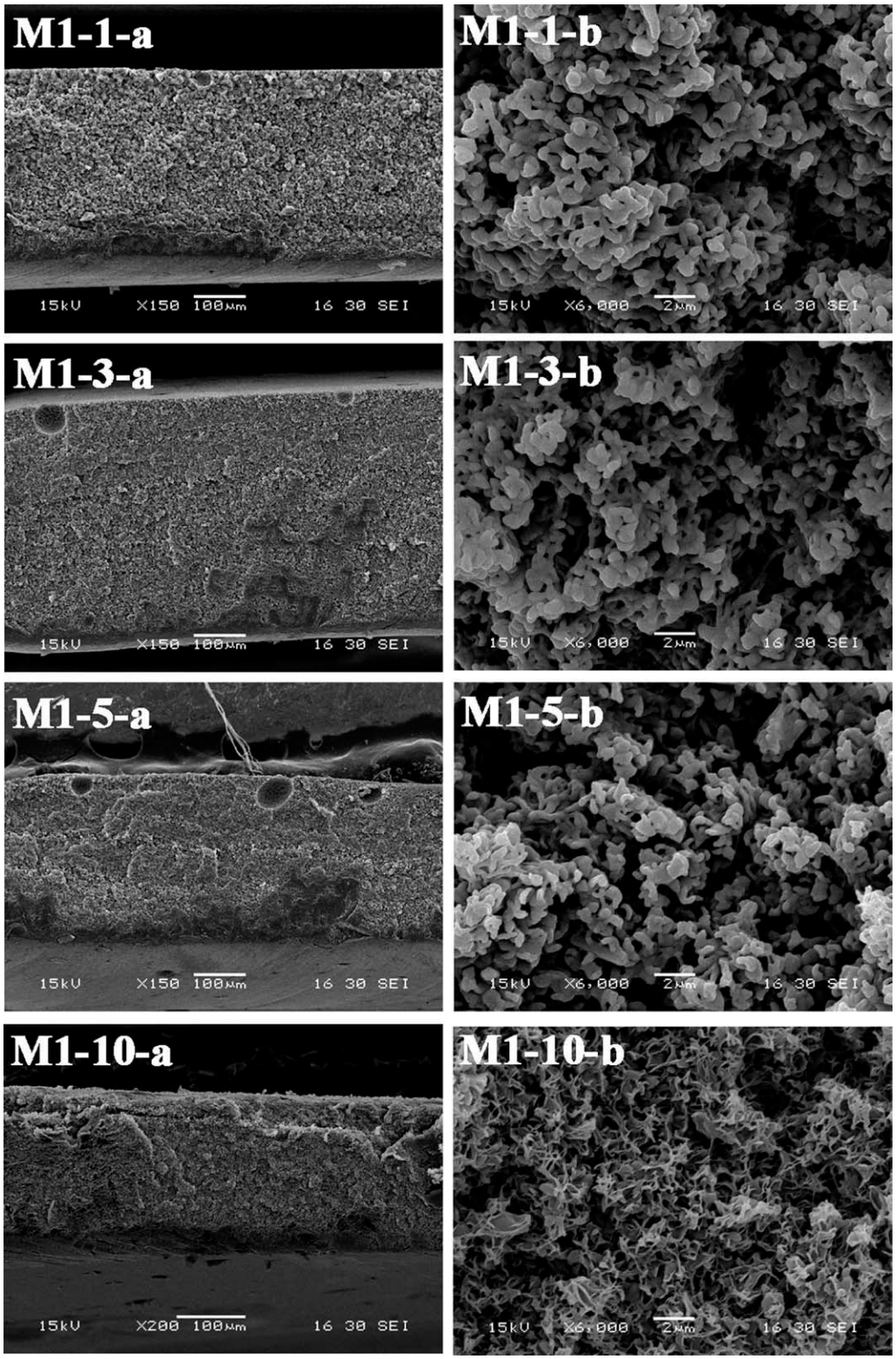

Figure 5. SEM micrographs of PVDF membranes with different nucleating agent contents: (a) whole and (b) enlarged cross sections.

M2 and M3 were the largest among all of the prepared membranes. The phenomenon corresponded to the higher flux values of M2 and M3. In addition, the mean pore size decreased with increasing TMB-5 content from 0.1 to 0.3 wt % and then increased with increasing TMB-5 content from 0.3 to 1.0 wt %. Membrane M1-3 had a minimum mean pore size value of 0.095 μm when the TMB-5 content was 0.3 wt %. Then, as shown in Figure 6, the pore size distribution of all of the membranes

Applied Polymer SCIENCE

Table III. Performances of the Different Membranes

Membrane	Nucleating agent Type	Content (wt %)	PWP ($L \cdot m^{-2} \cdot h^{-1}$)	Porosity (%)
M0	—	0	238	78.3
M1-1	TMB-5	0.1	191	78.8
M1-3	TMB-5	0.3	270	80.3
M1-5	TMB-5	0.5	111	75.4
M1-10	TMB-5	1.0	127	75.5
M2	TMP-1	0.3	297	70.3
M3	DM-LO	0.3	468	76.0

Table IV. Pore Sizes of the Different Membranes

Membrane	Nucleating agent Type	Content (wt %)	r_{max} (μm)	r_m (μm)	r_{min} (μm)
M0	—	0	0.183	0.140	0.089
M1-1	TMB-5	0.1	0.132	0.127	0.117
M1-3	TMB-5	0.3	0.105	0.095	0.085
M1-5	TMB-5	0.5	0.154	0.139	0.115
M1-10	TMB-5	1.0	0.186	0.135	0.119
M2	TMP-1	0.3	0.258	0.236	0.204
M3	DM-LO	0.3	0.267	0.236	0.199

prepared with nucleating agent was narrower than that of membrane M0 (without nucleating agent), although the pore sizes of membranes M2 and M3 were larger than that of M0. We concluded that the addition of nucleating agent led to a narrower pore size distribution, and when the addition amount of TMB-5 was 0.3 wt %, a minimum mean pore size value was obtained.

In conclusion, the nucleating agents TMP-1 and DM–LO were not suitable for preparing PVDF membranes via TIPS, although membranes M2 and M3 showed higher PWP values because membranes M2 and M3 had larger mean pore sizes, which meant lower rejection abilities. To the contrary, the nucleating agent TMB-5 was suitable because membrane M1-3 had a homogeneous, interconnected, bicontinuous structure, a minimum mean pore size and a higher porosity and PWP.

CONCLUSIONS

PVDF microporous membranes with interconnected, bicontinuous structures were successfully prepared by the TIPS method with the nucleating agent TMB-5 as an additive. The results reveal that the type and content of nucleating agent had no clearly effect on the thermodynamics of phase separation. However, the crystallization dynamics of S–L phase separation were affected by the addition of nucleating agent. As to the three nucleating agents (TMB-5, TMP-1, and DM–LO), the system with TMB-5 had the fast crystallization rate and a better nucleation ability, and a suitable dosage was 0.3 wt %.

The membrane structure changed with the addition of nucleating agent. With a 0.3 wt % content of nucleating agent, the membranes with TMP-1 and DM–LO showed partly closed, lacy bicontinuous structures. As the TMB-5 content increased,

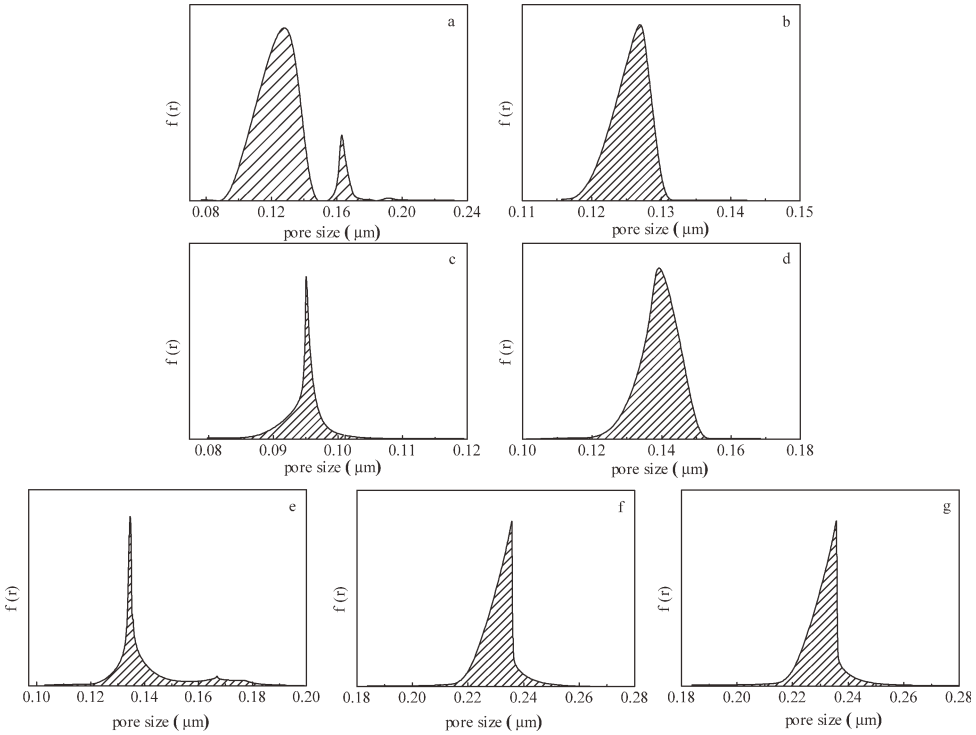

Figure 6. Pore size distributions of different membranes: (a) M0, (b) M1-1, (c) M1-3, (d) M1-5, (e) M1-10, (f) M2, and (g) M3.

the membrane structure changed from a bicontinuous structure with small deformation spherulites (0.1 wt %) to an interconnected, bicontinuous structure (0.3 wt %) and then transformed to a partly closed, lacy bicontinuous structure (1.0 wt %). With regard to the control of the membrane structure, TMB-5 acted as a good nucleating agent, and a suitable amount was 0.3 wt %.

The performances of the membranes were also affected by the nucleating agent. The nucleating agents TMP-1 and DM–LO were not suitable for preparing PVDF membranes via TIPS because the prepared membranes had mean pore sizes that were too large. The nucleating agent TMB-5 was suitable because the membrane had a minimum mean pore size (0.095 μm), higher porosity (80.3%), and PWP (270 $L{\cdot}m^{-2}{\cdot}h^{-1}$) at the addition content of 0.3 wt %. In addition, the addition of nucleating agent led to a narrower pore size distribution. The performances of the PVDF membrane with 0.3 wt % TMB-5 were much better than those of the pure PVDF membrane.

REFERENCES

1. Castro, A. J. U.S. Pat. 4,247,498 (**1981**).
2. Lloyd, D. R.; Kinzer, K. E.; Tseng, H. S. *J. Membr. Sci.* **1990,** *52*, 239.
3. Lloyd, D. R.; Kim, S. S.; Kinzer, K. E. *J. Membr. Sci.* **1991,** *64*, 1.
4. Kim, S. S.; Lloyd, D. R. *J. Membr. Sci.* **1991,** *64*, 13.
5. Lim, G. B. A.; Kim, S. S.; Ye, Q. H.; Wang, Y. F.; Lloyd, D. R. *J. Membr. Sci.* **1991,** *64*, 31.
6. Kim, S. S.; Lim, G. B. A.; Alwattari, A. A.; Wang, Y. F.; Lloyd, D. R. *J. Membr. Sci.* **1991,** *64*, 41.
7. Matsuyama, H.; Teramoto, M.; Kudari, S.; Kitamura, Y. *J. Appl. Polym. Sci.* **2001,** *82*, 169.
8. Matsuyama, H.; Maki, T.; Teramoto, M.; Asano, K. *J. Membr. Sci.* **2002,** *204*, 323.
9. Matsuyama, H.; Okafuji, H.; Maki, T.; Teramoto, M.; Kubota, N. *J. Membr. Sci.* **2003,** *223*, 119.
10. Matsuyama, H.; Hayashi, K.; Maki, T.; Teramoto, M.; Kubota, N. *J. Appl. Polym. Sci.* **2004,** *93*, 471.
11. Fu, X.-Y.; Matsuyama, H.; Teramoto, M.; Nagai, H. *Sep. Purif. Technol.* **2005,** *45*, 200.
12. Gu, M.-H.; Zhang, J.; Wang, X.-L.; Tao, H.-J.; Ge, L. *Desalination* **2006,** *192*, 160.
13. Gu, M.-H.; Zhang, J.; Wang, X.-L.; Ma, W.-Z. *J. Appl. Polym. Sci.* **2006,** *102*, 3714.
14. Cui, Z.-Y.; Du, C.-H.; Xu, Y.-Y.; Ji, G.-L.; Zhu, B.-K. *J. Appl. Polym. Sci.* **2008,** *108*, 272.
15. Yang, J.; Li, D.-W.; Lin, Y.-K.; Wang, X.-L.; Tian, F.; Wang, Z. *J. Appl. Polym. Sci.* **2008,** *110*, 341.
16. Ji, G.-L.; Du, C.-H.; Zhu, B.-K.; Xu, Y.-Y. *J. Appl. Polym. Sci.* **2007,** *105*, 1496.
17. Rajabzadeh, S.; Maruyama, T.; Sotani, T.; Matsuyama, H. *Sep. Purif. Technol.* **2008,** *63*, 415.
18. Ji, G.-L.; Zhu, B.-K.; Zhang, C.-F.; Xu, Y.-Y. *J. Appl. Polym. Sci.* **2008,** *107*, 2109.
19. Li, X.-F.; Xu, G.-Q.; Lu, X.-L.; Xiao, C.-F. *J. Appl. Polym. Sci.* **2008,** *107*, 3630.
20. Ji, G.-L.; Zhu, L.-P.; Zhu, B.-K.; Zhang, C.-F.; Xu, Y.-Y. *J. Membr. Sci.* **2008,** *319*, 264.
21. Liu, M.; Xu, Z.-L.; Li, J.-F.; Wu, X.-H. *Gongneng Gaofenzi Xuebao* **2009,** *22*, 88 (in Chinese).
22. Liu, M.; Xu, Z.-L.; Chen, D.-G.; Wei, Y.-M. *Desalination Water Treatment* **2010,** *17*, 183.
23. Deeprasertkul, B. S.·C. *J. Polym. Environ.* **2011,** *19*, 288.
24. Cramez, M. C.; Oliveira, M. J.; Carwford, R. J. *J. Mater. Sci.* **2001,** *36*, 2151.
25. McGuire, K. S.; Lloyd, D. R.; Lim, G. B. A. *J. Membr. Sci.* **1993,** *79*, 27.
26. Luo, B.-Z.; Zhang, J.; Wang, X.-L.; Zhou, Y.; Wen, J. *Desalination* **2006,** *192*, 142.
27. Han, X.-T.; Ding, H.-Y.; Wang, L.-H.; Xiao, C.-F. *J. Appl. Polym. Sci.* **2008,** *107*, 2475.
28. Smith, S. D.; Shipman, G. H.; Floyd, R. M.; Feemyer, H. T.; Hamrock, S. J.; Yandrasits, M. A.; Walton, D. G. S. U.S. Pat. 0,113,242 (**2008**).
29. Chen, G.-E.; Xu, Z.-L.; Shi, Y.-J. *J. East. Chin. Univ. Sci. Technol.* **1998,** *24*, 510 (in Chinese).
30. ASTM Standard F 316; Standard Test for Pore Size Characteristics of Membrane Filters by Bubble Point and Mean Flow Test; ASTM International: West Conshohocken, PA, **1986.**
31. McGuire, K. S.; Lawson, K. W.; Lloyd, D. R. *J. Membr. Sci.* **1995,** *99*, 127.
32. Venkataraman, K.; Choate, W.; Torre, E. R.; Husung, R.; Batchu, H. R. *J. Membr. Sci.* **1988,** *39*, 259.
33. Munari, S.; Bottino, A.; Moretti, P.; Capannelli, G.; Becchi, I. *J. Membr. Sci.* **1989,** *41*, 69.